ARTICLE

Received 00th January 20xx,

Accepted 00th January 20xx

DOI: 10.1039/x0xx00000x

Phenol is a pH-activated linker to gold: a single molecule conductance study

Brent Lawson,[a] Hannah E. Skipper[b], Maria Kamenetska [a,b,c]

Single molecule conductance measurements typically rely on functional linker groups to anchor the molecule to the conductive electrodes through a donor-acceptor or covalent bond. While many linking moities, such as thiols, amines, thiothers and phosphines have been used among others, very few involve oxygen binding directly to gold electrodes. Here, we report successful single molecule conductance measurements using hydroxy (OH)-containing phenol linkers and show that the molecule-gold attachment and electron transport is mediated by a direct O-Au bond. We find that deptrotonation of the hydroxy moiety is necessary for metal-molecule binding to proceed, so that junction formation can be activated through pH control. Electronic structure and DFT+Σ transport calculations confirm our experimental findings that phenolate-terminated alkanes can anchor on the gold and show charge transport trends consistent with prior observations of alkane conductance with other linker groups. Critically, the deprotonated O^--Au binding shows features similar to the thiolate-Au bond, but without the junction disruption caused by intercalation of sulfur into electrode tips often observed with thiol-terminated molecules. By comparing the conductance and binding features of O-Au and S-Au bonds, this study provides insight into the aspects of Au-linker bonding that promote reproducible and robust single molecule junction measurements.

Introduction

A versatile toolbox of molecular components with diverse electronic transport and binding properties is a necessity for advancing the field of molecular electronics. Single molecule junction measurements such as scanning tunneling microscope break junctions (STMBJ) and mechanically controlled break junctions (MCBJ) have been widely used to understand the ballistic transport of electrons through different families of molecules bound to atomic-scale electrodes, which are typically gold (Au), silver (Ag), or platinum (Pt).[1–9] Single molecules can bridge the source-drain gap by binding to the electrodes through chemical linker groups.[10–13] The nature of the metal electrode and hard-soft acid-base principles from synthetic chemistry determine the types of the metal-linker group interactions that enable successful single molecule junction formation.[14] For example, Au, which is the most used electrode material, is synthetically "soft" and thus forms strong covalent bonds with the "soft", polarizable sulfur linker groups. Thiol-terminated molecules result in molecular junctions with disrupted Au-Au interactions due to intercalation of sulfur into electrode tips and disperse molecular conductance signatures which can make it challenging to quantify conductance trends.[15] Linker groups which are intermediate on the hard-soft continuum, such as imines and amines, bind to the gold electrode via a dative interaction.[3,16–34] Weaker than a covalent bond, this donor-acceptor interaction does not disrupt Au-Au interactions and is also selective for specific binding geometries, limiting dispersion in single molecule conductance signatures on gold.[3,12,13] Notably, a certain number of donor linker groups such as the pyrrole nitrogen on imidazole require deprotonation in basic conditions to enable binding to the electrode.[21,23,37–39]

In contrast to sulfur, oxygen is understood to be a "hard" donor atom. Although in the same chalcogen group as sulfur one row below it in the period table, oxygen is known as an unfavorable binding linker to the "soft" metals like Au and Pt.[40] Compared to sulfur, relatively few examples of oxygen-gold bonds are known in the inorganic synthetic literature, though recently phenols were found to bind to Au surfaces to form self-assembled monolayer with similar properties to thiols.[41] The few examples of oxygen-metal (O-M) binding in single molecule junction studies typically involve two binding moieties to form bidentate links such as with amides or with carboxyl groups to strengthen the metal-molecule interaction.[37,39,42–45] The specific monodentate O-M binding with a hydroxy group such as alcohol, phenol or ether group have not been observed in a molecular junction for conductance measurements on gold.

In this paper we discover that O-Au binding can be realized in a single molecule junction through pH control which activates the oxygen on a phenol moiety for linking to gold electrodes. The resulting phenolate-bound molecules show

[a] Department of Physics, Boston University, Boston, Massachusetts, 02215, United States.
[b] Department of Chemistry, Boston University, Boston, Massachusetts, 02215, United States.
[c] Division of Material Science and Engineering, Boston, Massachusetts, 02215, United States.

Electronic Supplementary Information (ESI) available: [details of any supplementary information available should be included here]. See DOI: 10.1039/x0xx00000x

robust single molecule conductance features. Alcohols which have a pKa higher than 14 cannot be deprotonated and activated to bind in aqueous conditions. We study the conductance of a series of phenol-terminated amino alkanes deprotonated at pH > 10 and dried on gold samples prior to junction formation. We find that the conductance decays exponentially and molecular junction persistence grows linearly with molecule length as expected, confirming that transport is occurring through the phenolate-bound molecular backbone. Our density functional theory (DFT) and Non-Equilibrium Greens Function (NEGF) calculations show that conductance through phenolate-terminated molecules is mediated by the highest occupied molecular orbital (HOMO). Using the DFT+Σ formalism, we accurately predict the tunneling transport characteristics of these systems. Overall, we find that O-Au binding is a promising linking strategy for environmentally controlled and robust molecular junctions. Importantly, our combined experimental and computational measurements on this novel linker system allow us to develop important insights into linker features conducive to effective anchoring on gold for molecular electronics and interface functionalization applications.

Methods

Break Junction Measurements

Break junction measurements are performed using a homebuilt STMBJ previously described in detail.[2,3,29] The conductance measurements are made by bringing an Au tip repeatedly in and out of contact with an Au substrate at 16 nm/s, at a fixed bias below 500 mV. All conductance measurements were repeated at a range of bias voltages below 500 mV to verify no bias dependence for the molecules probed here in this regime. These results are show in the ESI in Fig. S1-4. The pull-out portion of each cycle is recorded at 40 kHz and constitutes an individual conductance trace. Measurements in the presence of molecules are done either in solution or with molecules dried on the surface using the drop casting method as previously detailed and discussed in the ESI.[23] We verify that conductance histograms measured in aqueous conditions with a wax-coated tip agree with the dried measurements when the molecules are deposited on samples out of solution as shown in Fig. S5.[46] All molecules, solvents and Au wire are purchased from Sigma-Aldrich.

Conductance histograms are constructed out of a minimum of 5000 individual conductance traces. We bin the logarithm of all recorded traces without any data selection. 2D Histograms bin both conductance and displacement. The zero of displacement in each trace is defined as the Au-Au rupture point when the conductance drops below the metallic regime (1 G_0) to the molecular scale.

Theoretical Calculations

All DFT calculations are performed with FHI-aims to obtain relaxed atomic-scale structures as well as binding energies and configurations.[47,48] All calculations in FHI-aims are performed using the PBE exchange correlation functional with "tight" level basis set.[49] Each molecule was relaxed initially in a fully extended conformer and converged to the lowest energy state. The molecule was then bound between two Au_{34} electrodes and the lowest energy junction distance was found by moving the electrodes in and out in steps of 0.05 Å. During each step, all atoms associated with the molecule as well as the four apex atoms for each electrode were allowed to relax, leaving the Au atoms in the final three rows frozen. This procedure identifies the most stable junction structures and equilibrium bond lengths.

The interatomic potential for the O-Au bond is calculated by starting from the lowest energy geometry found above and stretching and compressing the O-Au distance in steps of 0.1 Å keeping all other relative atom positions frozen and running a single Self Consistent Field Energy calculation at each step. The total energy was scaled for each system to 0 eV at O-Au bond lengths of ~5.0 Å (broken bond) to remove long range effects in the charged systems. Each interatomic potential scan is fit to a Morse potential $V(r)$, given by the fitting function:

$$V(r) = D_e\left(e^{-2a(r-R_e)} - 2e^{-a(r-R_e)}\right)$$

where r is the O-Au bond length at each step in the scan, D_e is the well depth, a is the width of the potential and R_e is the equilibrium bond length.[50,51]

Transmission of the metal-molecule-metal junction is calculated using a combination of NEGF as implemented in AITRANSS with adjustments based on DFT+Σ.[35,52–58] All transmission spectra calculated here using NEGF overestimated the conductance by more than an order of magnitude due to the presence of a HOMO resonance near the Fermi energy (E_F). DFT+Σ is implemented to shift the resonance away from E_F by accounting for self-interaction energy errors and image charge effects. The DFT+Σ adjusted transmission at $E\text{-}E_F$=0 eV is calculated and reported from the single energy level approximation. The description of the method to calculate the reference HOMO energy level as well as other approximations required in DFT+Σ is described in detail in the ESI.

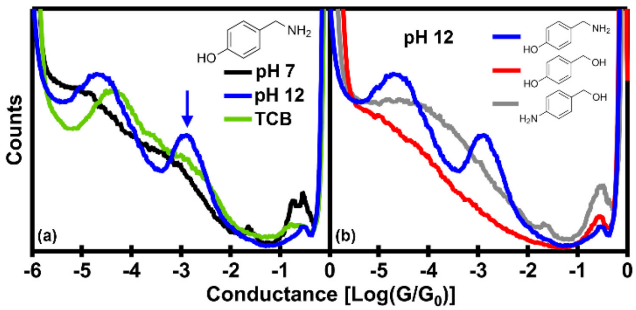

Fig. 1. (a) 1D conductance measurements of 4-hydroxybenzylamine in pH 7 (black) and pH 12 (blue) aqueous conditions, as well as 4-hydroxybenzylamine in trichlorobenzene (green). **(b)** 1D Conductance measurements of 4-hydroxybenzylamine (blue), 4-hydroxybenzyl alcohol (red), and 4-aminobenzyl alcohol (gray) in pH 12 aqueous conditions.

Results & Discussion

Experimental Measurements

Conductance histograms of 4-hydroxybenzylamine (NH_2C_1PhOH) depicted in the inset of Fig. 1a, measured in various solvent conditions are shown in Fig. 1a. NH_2C_1PhOH, consists of a phenyl ring terminated by a hydroxy group on one end, forming a phenol, and a methylamine (NH_2C1) on the other, with the NH_2 amine electron donor group terminating the molecule. No successful conductance measurements on a phenol have been reported in the literature to date. Our data in aprotic organic solvent 1,2,4-trichlorobenzene (TCB), plotted in green, are consistent with these prior findings, and show only a broad peak below 10^{-4} G_0. Such dispersed low conductance peaks have been previously attributed to aromatic molecules containing only one functional linker group, in this case the amine, anchoring to opposite electrodes and π-π stacking in the junction.[59,60] Here, we see that the feature is particularly pronounced in TCB, but is nearly absent in pH 7 aqueous conditions, shown in black. In TCB, amines are neutral and can bind in the junction to create π-π stacked dimer junctions, while in neutral water, the amine (pKa ~9) is likely to be protonated and unable to anchor the molecule.[43] We verify this fact by measuring 1,4-benzenediamine, a standard aromatic diamine control,[3] dissolved in pH 7 water and observe no conductance signals as shown in the ESI Fig. S6. In pH 7 the phenol (pKa ~10) also remains protonated and does not bind, preventing the formation of through-bond conductance signatures with a single molecule bound to both electrodes.

Importantly, however, measurements of NH_2C_1PhOH in basic conditions, shown in blue in Fig. 1a, lead to the appearance of a distinct feature at a higher conductance regime indicated by an arrow and consistent with a single molecule signature where both ends are anchored to opposite electrodes. We compare these measurements on NH_2C_1PhOH to the conductance of an analogous diamine, 5-aminobenzilamine (5ABA), where the OH group is replaced by an amine. The results are plotted in Figure S6 and show that both the single molecule and the π-π stacked peak are similar in the two molecules, but the phenol has a somewhat higher conductance than the amine. We note that in pH 12 aqueous conditions, both the amine (pKa ~9) and the phenol (pKa ~10) are deprotonated so that the amine is neutral, and the phenol group becomes charged ($NH_2C_1PhO^-$). These results suggest that the deprotonated phenol moiety, phenolate, can bind to gold to bridge metal-molecule junctions.

To understand which conditions, enable O-Au binding, we perform measurements, shown in Fig. 1b, on two control molecules, 4-hydroxybenzyl alcohol (red) and 4-aminobenzyl alcohol (gray) whose structures are shown in the inset. In both molecules, one of the linkers is a hydroxy moiety bound to a saturated chain (alcohol) rather than to an aromatic benzene (phenol). As a result, the pKa of these molecules is ~16, which is significantly higher than of a phenol and outside the accessible pH range with aqueous solvent. Fig. 1b makes clear that these molecules do not display a single molecule conductance feature, even at pH≳12 experimental conditions. We conclude that deprotonation is necessary to enable O-Au binding in the single molecule junction environment. Thus, a phenol with a pKa ~10 is a viable linker group for single molecule conductance measurements in aqueous conditions where it can be deprotonated to phenolate at pH > 10, but an alcohol with a pKa ~16, is not.

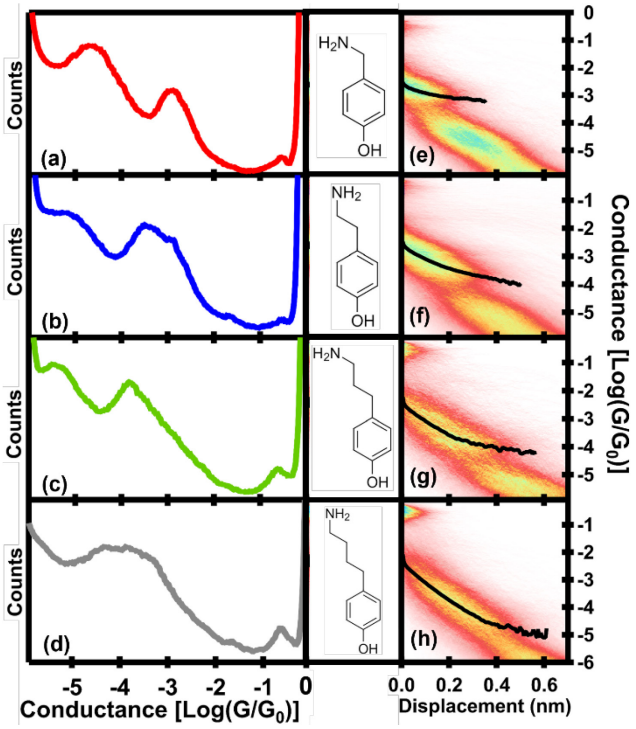

Fig. 2. 1D conductance histograms and 2D conductance vs displacement histograms of $NH_2C_1PhO^-$ **(a, e),** $NH_2C_2PhO^-$ **(b, f)**, $NH_2C_3PhO^-$ **(c, g)** and $NH_2C_4PhO^-$ **(d, h)**. The black line in **(e-h)** is the gaussian fit of each vertical slice in the 2D histogram. The line cuts off after the amplitude of the Gaussian fit falls off by 85% below the maximum.

To study the conductance characteristics of phenolate (PhO^-) as a linker group in break junction measurements, we measure the conductance decay of the series of alkanes, ranging in length from 1 to 4 methylene groups (C_1 = $-CH_2-$, C_2 = $-(CH_2)_2-$, C_3 = $-(CH_2)_3-$, C_4 = $-(CH_2)_4-$), terminated by PhO^- (measured in pH 12) and an amine, shown in Fig 2. We refer to these molecules as NH_2C_nPhO-, where n ranges from 1 to 4. Each of the 1D conductance histograms (Fig. 2a-d), comprised of at least 5,000 individual pull-out conductance traces for all four molecules shows a pronounced single molecule conductance feature. This peak is higher in conductance than the π-π stacking feature which is present in all molecules except in $NH_2C_4PhO^-$ where it

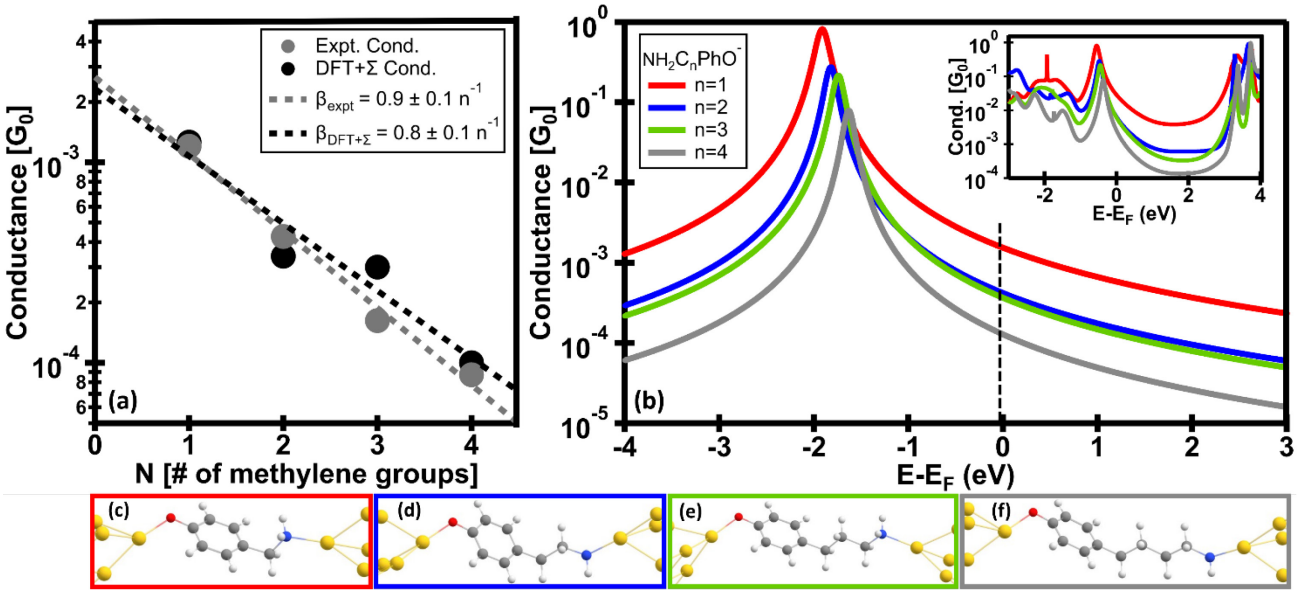

Fig. 3. (a) Comparison of the experimentally determined and DFT+Σ calculated conductance values of $NH_2C_nPhO^-$ (n=1-4) including the exponential fit for both and the corresponding parameters. **(b)** DFT+Σ adjusted single level HOMO resonance involved in transmission calculated at $E-E_F=0$ eV (dashed black line) for $NH_2C_nPhO^-$ (n=1-4). **(b, inset)** Initial transmission spectra calculated using NEGF. (c-f) Visualization of the lowest energy geometries of $NH_2C_nPhO^-$ (n=1-4) bound to two Au_{34} electrodes that are used for transmission calculations.

falls below the measurement noise floor. We track the characteristic conductance of each molecule by fitting the peak to a Gaussian fit and determine the average conductance of $NH_2C_1PhO^-$, $NH_2C_2PhO^-$, $NH_2C_3PhO^-$, $NH_2C_4PhO^-$ to be $10^{-2.92}$, $10^{-3.37}$, $10^{-3.80}$, and $10^{-4.06}$ G_0 respectively.

The 2D conductance vs. displacement histogram for these four alkanes is shown in Fig. 2e-h and provides information on the relative length of the molecular junction as well as how the conductance traces evolve during junction stretching. The black lines trace the average conductance at each junction extension determined via a Gaussian fit to a vertical slice of the 2D histogram. The extension where the Gaussian fits diminish by 85% of the peak amplitude is identified by the end of the black line and is interpreted as a representative length of a fully elongated molecular junction prior to junction rupture. The junction persistence lengths as well as junction formation probability determined for all molecules using molecular plateau length analysis techniques is shown in ESI Fig. S7 and provides similar results.[61] Using both types of measurements, we find that as the number of methylene groups increases, the persistence of the molecular junctions grows, so that average junction breakdown occurs at longer extensions between the electrodes. We observe a persistence length of ~3Å for $NH_2C_1PhO^-$ and ~6 Å for $NH_2C_4PhO^-$ indicating that these molecules are fully elongated in the junction after stretching of 3 and 6 Å, respectively, beyond metallic rupture. Accounting for Au electrode relaxation (snapback) of ~5 Å that occurs when gold point contacts break down and separate,[8,61,62] these lengths are consistent with the calculated molecular junction lengths of ~8 Å and ~11 Å for $NH_2C_1PhO^-$ and $NH_2C_4PhO^-$ respectively. Importantly, we find that the persistence of $NH_2C_1PhO^-$ and 4ABA, an analogous amine, molecular junctions are very similar (Figure S6b). Molecule and junction lengths of all molecules studied here are listed in the ESI in Tables S5 and S6. In all cases, the extension lengths and persistence probabilities plotted in Figures 2 and S7 are consistent with measurements done on conjugated diamine and carboxyl-linked molecules of similar length reported previously, suggesting that the phenolate-bound junctions are comparable in stability to other commonly used linkers.[29,30,37,63] These results and analysis confirm that the electrode binds to the fully extended molecule at the oxygen contact and not through van der Waals interaction with the phenyl ring which would result in shorter persistence in the junction.

To understand how the phenolate linker group effects conductivity through the alkane backbone, we plot the characteristic conductance values obtained from Gaussian fits of the 1D conductance histograms in Fig 2a-d, against the number of methylene groups, N in Fig. 3a (gray). We observe a characteristic exponential decay with increasing number of methylene groups, which is a well-documented feature of off resonance tunneling in single molecule junctions. Using common practice, we fit the data with an exponential decay $R_C{}^{-1}e^{-\beta N}$, where β is the decay rate and R_c is the contact resistance of the two ends of the molecule. The experimental conductance decay rate, β_{expt}, is determined to be $\beta_{expt} = 0.9 \pm 0.1$ per methylene. The value of β_{expt} matches previous measurements for an alkane backbone which range from 0.8 to 1.1.[3,31,36,64–66] The measured R_c of the phenol linker is 4.5 MΩ, where we account for the R_c of the amine to be 215 kΩ as previously measured.[3] We note that the phenol R_c is comparable in magnitude to the R_c of similar linker groups such

as pyridine, thiophenol and thioanisole, which are 1.9, 3.8-5.5, and 9 MΩ respectively.[66–68] The agreement between our measured R_c for the phenol and previously measured thiophenol further confirms that our single molecule conductance signatures are from direct O-Au binding and suggests that the electronic resistance characteristics of S-Au and O-Au links are similar.

Theoretical Calculations

To investigate the binding configuration and electronic structure of phenolate terminated molecular junctions we relax each of the four alkane phenolates studied here bound to Au_{34} electrodes (Fig. 3c-f) in the fully extended but still stable configuration (see Methods). The Au-Au separation (edge-to-edge) in the order of increasing molecule lengths are found to be 7.6, 8.6, 10.1, and 11 Å which is consistent with the overall lengths and successive addition of a methylene group.[3] We calculate the expected electron transport of the four junctions using NEGF method from Kohn-Sham DFT (KS-DFT). The calculated transmission spectra for all four junctions are shown in the inset in Fig. 3b. We observe that the calculated low bias transmission evaluated at $E\text{-}E_F = 0$ eV for all four junctions is $\gtrsim 10^{-2}G_0$, several orders of magnitude higher than the experimentally measured conductance plotted in Fig. 3a. We also find that the HOMO resonance is predicted to be within only ~0.5 eV of E_F. This resonance near E_F magnifies effects of the known DFT underestimation of the HOMO-LUMO gap and results in a drastic overestimation of conductance.

To improve the accuracy of our calculation, we turn to DFT+Σ method to estimate the transmission. This method is well-suited to situations where conductance is dominated by a single resonance, in this case, the HOMO. The LUMO, at more than 3.5 eV away, can be neglected. The full DFT+Σ analysis is shown in the ESI for all molecules and junction geometries considered here. The DFT+Σ predicted HOMO resonance position and width for all four molecular junctions is represented by a Lorentzian curve plotted relative to $E\text{-}E_F$ in Fig. 3b**.** We find that the DFT+Σ correction shifts the resonance for all molecules $NH_2C_1PhO^-$, $NH_2C_2PhO^-$, $NH_2C_3PhO^-$, $NH_2C_4PhO^-$ by ~1.3 eV away from the Fermi energy to -1.91, -1.82, -1.74, -1.63 eV, respectively. This shift of the HOMO in the DFT+Σ comes from two distinct contributions: the gas-phase correction and image charge correction.[58] Notably, we find the gas-phase correction for the four molecules is approximately -2.2 eV, which is significantly larger than is typical for neutral systems and emphasizes the need for DFT+Σ correction for this case. We note that the large offset found here for phenolates PhO^- reflects the documented difficulty of KS-DFT to predict the energy levels of anions, which exacerbates the standard HOMO-LUMO gap underestimation of DFT methods.[69–71] We note that further work on charged molecular junctions may require the DFT+Σ methodology detailed and validated here for anions bound to two electrodes.

We compare the calculated conductance values, obtained by evaluating the transmission in Fig. 3b at E_F and plotted in Fig. 3a (black), with experimental measurements (gray). We observe

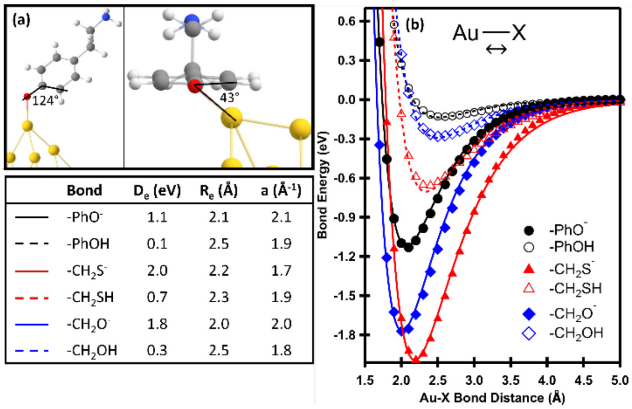

Bond	D_e (eV)	R_e (Å)	a (Å^{-1})
-PhO$^-$	1.1	2.1	2.1
-PhOH	0.1	2.5	1.9
-CH$_2$S$^-$	2.0	2.2	1.7
-CH$_2$SH	0.7	2.3	1.9
-CH$_2$O$^-$	1.8	2.0	2.0
-CH$_2$OH	0.3	2.5	1.8

Fig 4. (a) Binding configuration of Au_{34}- $NH_2C_2PhO^-$. **Table 1.** Morse Potential Fitting Parameters determined from Fig. 4a [well depth (D_e), equilibrium bond length (R_e), well width (a)]. (b) Potential energy scan against length of the Au-X (X=PhO^-, PhOH, CH_2S^-, CH_2SH, CH_2O^-, CH_2OH) bond, with Au electrode modelled as Au_{34}. The Au apex atom is bound to either O or S in all cases. Data points were fit with Morse potential function, plotted as solid lines.

strong agreement for all four molecular junctions; the DFT+ Σ-calculated decay $\beta_{DFT+\Sigma}$ falls within the statistical uncertainty of the measured β_{expt}, validating the application of this method to charged molecular junctions.

We examine the character of the PhO^--Au bond by studying the geometry of the $NH_2C_2PhO^-$-Au_{34} interface, shown in Fig. 4a. We observe a ~124° angle between Au-O-C (left) with the Au-O bond rotated ~45° clockwise relative to the plane of the phenyl ring (right). These observations indicate that a distortion from the original sp^2 hybridization of the phenolate to sp^3 occurs upon binding to gold. These changes in the electron distribution and local density of states are characteristic of a strong physisorption interaction or even of chemisorption.[72–75]

The strong nature of the binding is also evident in the calculated Morse potential shown in Fig. 4b (solid markers). The well depth or interaction energy (D_e), and equilibrium bond length (R_e) for PhO^- are 1.1 eV and 2.1 Å respectively. This is significantly stronger than the 0.6 eV dative donor acceptor interaction of amines to undercoordinated Au atoms commonly used in STMBJ measurements.[30,35,76] Interestingly, the Morse potential fit for a deprotonated alcohol (CH_2O^-) binding to Au shows an even stronger bond at 1.8 eV, but it is not observed in experiment due to the high pKa of alcohol which makes deprotonation impossible in aqueous conditions. Importantly, we also note that a protonated phenol (PhOH) or alcohol (CH_2OH) has a binding energy of 0.1 or 0.3 eV respectively, which is insufficient for stable junction formation at room temperature.

Interestingly, we see in Fig. 4b that the interaction strength of thiolate (CH_2S^-) at 2.0 eV is comparable to the alcohol interaction. The thiols in Fig. 4b are alkyl thiols, but similar analysis and results were obtained with thiophenols, as shown in Fig. S9 and Table S9. Critically, unlike the weak binding of OH, the SH moiety binds to gold with an appreciable binding energy of 0.7eV. These calculations support recent measurements

which show that thiol can retain the proton during junction formation and stretching at room temperature.[77] We conclude that while hydroxy moieties need to be activated through environmental removal of the proton in order to bind, the thiol will bind even in its protonated state. This donor-acceptor interaction of the protonated thiol may then be converted to a covalent bond between thiolate and gold which leads to disruptive intercalation of the thiolate into the electrode structure and the broadening of gold and molecular conductance signatures.[15]

These differences between phenol and thiol Au interactions are instructive for future design of linker moieties. Our results suggest that in addition to the energetics of the final binding configuration, which are similar for the S-Au and O-Au cases, the transition state energy and the existence of intermediate stable binding configurations are important to consider. Unlike thiolates, phenolates discovered here bind strongly, but non-destructively. The lack of a stable intermediate binding configuration between the neutral protonated phenol and the gold, prevents binding in neutral conditions and results in a linker which binds strongly and can be activated using environmental pH.[15,78]

Conclusions

Our results here show that a phenol group can be used as an affective linker group for metal-molecule junctions and is activated for binding in aqueous conditions through external pH control. Our break junction measurements show a single conductance signature associated with binding to Au electrodes via the deprotonated oxygen in a phenol that is not present when phenol or alcohol is protonated. Measurements with a series of alkanes using the phenolate as a linker group match the expected alkane conductance decay with molecule length. The calculated electron transport through the series of alkane phenolates anchored on gold with direct O-Au links, matches experiment when DFT+Σ adjustments are made to the HOMO dominated transmission spectra. We show that the Au-phenolate interaction has characteristics similar to the Au-thiolate bond but is more selective for binding configurations where the proton is removed. This selectivity results in the ability to control binding through external environment and reduces intercalation into the gold electrodes characteristic of thiol-linked junctions. This study of a new robust linker group for molecular junction measurements offers insight into features of metal-molecule interactions necessary for successful junction formation and opens the door to a broader range of molecular junctions and capabilities. This work points to an effective binding strategy for biological molecules rich in phenols, such as nucleic or amino acids, to gold surfaces without required labeling or modification for single molecule conductance, optical spectroscopy or other applications.

Conflicts of interest

There are no conflicts to declare.

Acknowledgements

This work was supported by the National Science Foundation under award # 2145276.

Notes and references

§
§§
etc.

1 M. A. Reed, C. Zhou, C. J. Muller, T. P. Burgin and J. M. Tour, *Science (80-.).*, 1997, **278**, 1–3.

2 B. Xu and N. J. Tao, *Science (80-.).*, 2003, **301**, 1221–1223.

3 L. Venkataraman, J. E. Klare, I. W. Tam, C. Nuckolls, M. S. Hybertsen and M. L. Steigerwald, *Nano Lett.*, 2006, **6**, 458–462.

4 J. C. Cuevas and E. Scheer, *Molecular Electronics: An Introduction to Theory and Experiment*, World Scientific Publishing Company, 2nd edn., 2017.

5 T. Kim, H. Vázquez, M. S. Hybertsen and L. Venkataraman, *Nano Lett.*, 2013, **13**, 3358–3364.

6 S. Kaneko, T. Nakazumi and M. Kiguchi, *J. Phys. Chem. Lett.*, 2010, **1**, 3520–3523.

7 M. Kiguchi, O. Tal, S. Wohlthat, F. Pauly, M. Krieger, D. Djukic, J. C. Cuevas and J. M. Van Ruitenbeek, *Phys. Rev. Lett.*, 2008, **101**, 1–4.

8 A. I. Yanson, G. Rubio Bollinger, H. E. Van Den Brom, N. Agraït and J. M. Van Ruitenbeek, *Nature*, 1998, **395**, 783–785.

9 N. Agraït, A. L. Yeyati and J. M. van Ruitenbeek, *Phys. Rep.*, 2003, **377**, 81–279.

10 T. A. Su, M. Neupane, M. L. Steigerwald, L. Venkataraman and C. Nuckolls, *Nat. Rev. Mater.*, , DOI:10.1038/natrevmats.2016.2.

11 C. A. Martin, D. Ding, J. Kryger Sørensen, T. Bjørnholm, J. M. van Ruitenbeek and H. S. J. van der Zant, *J. Am. Chem. Soc.*, 2008, **130**, 13198–13199.

12 E. Leary, A. La Rosa, M. T. González, G. Rubio-Bollinger, N. Agraït and N. Martín, *Chem. Soc. Rev.*, 2015, **44**, 920–942.

13 Z. L. Cheng, R. Skouta, H. Vazquez, J. R. Widawsky, S. Schneebeli, W. Chen, M. S. Hybertsen, R. Breslow and L. Venkataraman, *Nat. Nanotechnol.*, 2011, **6**, 353–357.

14 H. Skipper, C. May, A. Rheingold, L. Doerrer and M. Kamenetska, *J. Am. Chem. Soc.*, **143**, 16439–16447.

15 E. Leary, L. A. Zotti, D. Miguel, I. R. Márquez, L. Palomino-Ruiz, J. M. Cuerva, G. Rubio-Bollinger, M. T. González and N. Agrait, *J. Phys. Chem. C*, 2018, **122**, 3211–3218.

16 W. Chen, J. R. Widawsky, H. Vázquez, S. T. Schneebeli, M. S. Hybertsen, R. Breslow and L. Venkataraman, *J. Am. Chem. Soc.*, 2011, **133**, 17160–17163.

17 Y. Y. Sun, Z. L. Peng, R. Hou, J. H. Liang, J. F. Zheng, X. Y. S. Zhou, X. Y. S. Zhou, S. Jin, Z. J. Niu and B. W. Mao, *Phys. Chem. Chem. Phys.*, 2014, **16**, 2260–2267.

18 Z. W. Hong, M. A. Ben Aissa, L. L. Peng, H. Xie, D. L. Chen, J. F. Zheng, Y. Shao, X. S. Zhou, N. Raouafi and Z. J. Niu, *Electrochem. commun.*, 2016, **68**, 86–89.

19 W. Q. Li, B. Huang, M. L. Huang, L. L. Peng, Z. W. Hong, J. F. Zheng, W. B. Chen, J. F. Li and X. S. Zhou, *Sensors*

(Switzerland), 2017, **17**, 1–8.
20 S. V. Aradhya, M. Frei, A. Halbritter and L. Venkataraman, *ACS Nano*, 2013, **7**, 3706–3712.
21 C. P. Tao, C. C. Jiang, Y. H. Wang, J. F. Zheng, Y. Shao and X. S. Zhou, *J. Phys. Chem. Lett.*, 2020, **11**, 10023–10028.
22 A. Mishchenko, L. A. Zotti, D. Vonlanthen, M. Bürkle, F. Pauly, J. C. Cuevas, M. Mayor and T. Wandlowski, *J. Am. Chem. Soc.*, 2011, **133**, 184–187.
23 X. Pan, B. Lawson, A. M. Rustad and M. Kamenetska, *Nano Lett.*, 2020, **20**, 4687–4692.
24 C. Wu, A. Alqahtani, S. Sangtarash, A. Vezzoli, H. Sadeghi, C. M. Robertson, C. Cai, C. J. Lambert, S. J. Higgins and R. J. Nichols, *Nanoscale*, 2020, **12**, 7914–7920.
25 T. Fu, S. Smith, M. Camarasa-Gómez, X. Yu, J. Xue, C. Nuckolls, F. Evers, L. Venkataraman and S. Wei, *Chem. Sci.*, 2019, **10**, 9998–10002.
26 A. C. Whalley, C. Nokolls, H. J. Choi, J. B. Neaton, L. Venkataraman, M. Kamenetska, M. L. Steigerwald, M. S. Hybertsen, S. G. Louie and S. Y. Quek, *J. Am. Chem. Soc.*, 2010, **132**, 6817.
27 G. Pacchioni, *Nat. Rev. Mater.*, 2019, **4**, 226.
28 M. S. Hybertsen, L. Venkataraman, J. E. Klare, A. C. Whalley, M. L. Steigerwald and C. Nuckolls, *J. Phys. Condens. Matter*, 2008, **20**, 374115.
29 J. McNeely, N. Miller, X. Pan, B. Lawson and M. Kamenetska, *J. Phys. Chem. C*, 2020, **124**, 13427–13433.
30 Y. S. Park, A. C. Whalley, M. Kamenetska, M. L. Steigerwald, M. S. Hybertsen, C. Nuckolls and L. Venkataraman, *J. Am. Chem. Soc.*, 2007, **129**, 15768–15769.
31 R. Parameswaran, J. R. Widawsky, H. Vázquez, Y. S. Park, B. M. Boardman, C. Nuckolls, M. L. Steigerwald, M. S. Hybertsen and L. Venkataraman, *J. Phys. Chem. Lett.*, 2010, **1**, 2114–2119.
32 T. A. Su, H. Li, R. S. Klausen, N. T. Kim, M. Neupane, J. L. Leighton, M. L. Steigerwald, L. Venkataraman and C. Nuckolls, *Acc. Chem. Res.*, 2017, **50**, 1088–1095.
33 B. Capozzi, E. J. Dell, T. C. Berkelbach, D. R. Reichman, L. Venkataraman and L. M. Campos, *J. Am. Chem. Soc.*, 2014, **136**, 10486–10492.
34 F. Chen, L. L. Peng, Z. W. Hong, J. C. Mao, J. F. Zheng, Y. Shao, Z. J. Niu and X. S. Zhou, *Nanoscale Res. Lett.*, 2016, **11**, 1–5.
35 S. Y. Quek, L. Venkataraman, H. J. Choi, S. G. Louie, M. S. Hybertsen and J. B. Neaton, *Nano Lett.*, 2007, **7**, 3477–3482.
36 C. R. Arroyo, E. Leary, A. Castellanos-Gómez, G. Rubio-Bollinger, M. T. González and N. Agraït, *J. Am. Chem. Soc.*, 2011, **133**, 14313–14319.
37 S. Ahn, S. V. Aradhya, R. S. Klausen, B. Capozzi, X. Roy, M. L. Steigerwald, C. Nuckolls and L. Venkataraman, *Phys. Chem. Chem. Phys.*, 2012, **14**, 13841–13845.
38 Z. Li, M. Smeu, S. Afsari, Y. Xing, M. A. Ratner and E. Borguet, *Angew. Chemie - Int. Ed.*, 2014, **53**, 1098–1102.
39 B. Wu, W. Guo, J. An and H. Li, *J. Mater. Chem. C*, 2022, **10**, 13483–13498.
40 G. L. Miessler, P. J. Fischer and D. A. Tarr, *Inorganic Chemistry*, Pearson Education Inc., 5th edn., 2014.
41 S. Menachekanian, C. Mora Perez, A. K. Pennathur, M. J. Voegtle, D. Blauth, O. V. Prezhdo and J. M. Dawlaty, *J. Phys. Chem. Lett.*, 2023, 8353–8359.
42 M. Huang, Q. Zhou, F. Liang, L. Yu, B. Xiao, Y. Li, M. Zhang, Y. Chen, J. He, S. Xiao and S. Chang, *Nano Lett.*, 2021, **21**, 5409–5414.
43 F. Chen, X. Li, J. Hihath, Z. Huang and N. Tao, *J. Am. Chem. Soc.*, 2006, **128**, 15874–15881.
44 J. R. Huang, H. Huang, C. P. Tao, J. F. Zheng, Y. Yuan, Z. W. Hong, Y. Shao, Z. J. Niu, J. Z. Chen and X. S. Zhou, *Nanoscale Res. Lett.*, 2019, **14**, 253.
45 L. Tong, Z. Yu, Y. J. Gao, X. C. Li, J. F. Zheng, Y. Shao, Y. H. Wang and X. S. Zhou, *Nat. Commun.*, 2023, **14**, 3397.
46 L. A. Nagahara, T. Thundat and S. M. Lindsay, *Rev. Sci. Instrum.*, 1989, **60**, 3128–3130.
47 V. Blum, R. Gehrke, F. Hanke, P. Havu, V. Havu, X. Ren, K. Reuter and M. Scheffler, *Comput. Phys. Commun.*, 2009, **180**, 2175–2196.
48 X. Ren, P. Rinke, V. Blum, J. Wieferink, A. Tkatchenko, A. Sanfilippo, K. Reuter and M. Scheffler, *New J. Phys.*, , DOI:10.1088/1367-2630/14/5/053020.
49 J. P. Perdew, K. Burke and M. Ernzerhof, *Phys. Rev. Lett.*, 1996, **77**, 3865–3868.
50 P. M. Morse, *Phys. Rev.*, 1929, **34**, 57–64.
51 L. A. Girifalco and V. G. Weizer, *Phys. Rev.*, 1959, **114**, 687–690.
52 A. Arnold, F. Weigend and F. Evers, *J. Chem. Phys.*, , DOI:10.1063/1.2716664.
53 A. Bagrets, *J. Chem. Theory Comput.*, 2013, **9**, 2801–2815.
54 J. Wilhelm, M. Walz, M. Stendel, A. Bagrets and F. Evers, *Phys. Chem. Chem. Phys.*, 2013, **15**, 6684–6690.
55 J. B. Neaton, M. S. Hybertsen and S. G. Louie, *Phys. Rev. Lett.*, , DOI:10.1103/PhysRevLett.97.216405.
56 T. Markussen, C. Jin and K. S. Thygesen, *Phys. Status Solidi Basic Res.*, 2013, **250**, 2394–2402.
57 J. R. Widawsky, P. Darancet, J. B. Neaton and L. Venkataraman, *Nano Lett.*, 2012, **12**, 354–358.
58 E. Montes and H. Vázquez, *Appl. Sci.*, 2021, **11**, 1–12.
59 S. Wu, M. T. González, R. Huber, S. Grunder, M. Mayor, C. Schönenberger and M. Calame, *Nat. Nanotechnol.*, 2008, **3**, 569–574.
60 S. Martín, I. Grace, M. R. Bryce, C. Wang, R. Jitchati, A. S. Batsanov, S. J. Higgins, C. J. Lambert and R. J. Nichols, *J. Am. Chem. Soc.*, 2010, **132**, 9157–9164.
61 C. Untiedt, A. I. Yanson, R. Grande, G. Rubio-Bollinger, N. Agraït, S. Vieira and J. M. van Ruitenbeek, *Phys. Rev. B - Condens. Matter Mater. Phys.*, 2002, **66**, 854181–854186.
62 M. Kamenetska, M. Koentopp, A. C. Whalley, Y. S. Park, M. L. Steigerwald, C. Nuckolls, M. S. Hybertsen and L. Venkataraman, *Phys. Rev. Lett.*, 2009, **102**, 126803.
63 A. Mishchenko, D. Vonlanthen, V. Meded, M. Bürkle, C. Li, I. V. Pobelov, A. Bagrets, J. K. Viljas, F. Pauly, F. Evers, M. Mayor and T. Wandlowski, *Nano Lett.*, 2010, **10**, 156–163.
64 H. Li, M. H. Garner, T. A. Su, A. Jensen, M. S. Inkpen, M. L. Steigerwald, L. Venkataraman, G. C. Solomon and C. Nuckolls, *J. Am. Chem. Soc.*, 2017, **139**, 10212–10215.
65 X. Li, J. He, J. Hihath, B. Xu, S. M. Lindsay and N. Tao, ,

DOI:10.1021/ja057316x.
66 R. S. Klausen, J. R. Widawsky, M. L. Steigerwald, L. Venkataraman and C. Nuckolls, *J. Am. Chem. Soc.*, 2012, **134**, 4541–4544.
67 M. Gulcur, P. Moreno-García, X. Zhao, M. Baghernejad, A. S. Batsanov, W. Hong, M. R. Bryce and T. Wandlowski, *Chem. - A Eur. J.*, 2014, **20**, 4653–4660.
68 Z. Li, T. H. Park, J. Rawson, M. J. Therien and E. Borguet, *Nano Lett.*, 2012, **12**, 2722–2727.
69 K. R. Bryenton, A. A. Adeleke, S. G. Dale and E. R. Johnson, *Wiley Interdiscip. Rev. Comput. Mol. Sci.*, 2023, **13**, 29–32.
70 F. Jensen, *J. Chem. Theory Comput.*, 2010, **6**, 2726–2735.
71 M. C. Kim, E. Sim and K. Burke, *Phys. Rev. Lett.*, 2013, **111**, 1–5.
72 S. P. Jarvis, S. Taylor, J. D. Baran, D. Thompson, A. Saywell, B. Mangham, N. R. Champness, J. A. Larsson and P. Moriarty, *J. Phys. Chem. C*, 2015, **119**, 27982–27994.
73 Q. Zhang, X. Zheng, G. Kuang, W. Wang, L. Zhu, R. Pang, X. Shi, X. Shang, X. Huang, P. N. Liu and N. Lin, *J. Phys. Chem. Lett.*, 2017, **8**, 1241–1247.
74 A. Ceccatto Dos Santos, N. Herrera-Reinoza, A. Pérez Paz, D. J. Mowbray and A. De Siervo, *J. Phys. Chem. C*, 2021, **125**, 17164–17173.
75 M. R. Safari, F. Matthes, K.-H. Ernst, D. E. Bürgler and C. M. Schneider, *Nanomaterials*, 2022, 12.
76 R. C. Hoft, M. J. Ford, A. M. McDonagh and M. B. Cortie, *J. Phys. Chem. C*, 2007, **111**, 13886–13891.
77 H. Li, T. A. Su, M. Camarasa-Gómez, D. Hernangómez-Pérez, S. E. Henn, V. Pokorný, C. D. Caniglia, M. S. Inkpen, R. Korytár, M. L. Steigerwald, C. Nuckolls, F. Evers and L. Venkataraman, *Angew. Chemie - Int. Ed.*, 2017, **56**, 14145–14148.
78 Y. Xue, X. Li, H. Li and W. Zhang, *Nat. Commun.*, 2014, **5**, 1–9.